CERN-PBC-REPORT-2024-002

15 August 2024
vera.cilento@cern.ch

A systematic effect in EDM rings due to radial offsets of electrostatic bendings and longitudinal magnetic fields

V. Cilento, C. Carli
CERN, CH-1211 Geneva, Switzerland

Keywords: cpEDM, frozen spin, hybrid ring, spin precession, systematic effect

Summary

Optimization and realistic estimates of the sensitivity of the measurement of charged particle Electric Dipole Moment (EDM) in storage rings require a good understanding of systematic errors that can contribute to a vertical spin build-up mimicking the EDM signal to be detected. A specific case of systematic effects due to offsets of electrostatic bendings and longitudinal magnetic fields is studied. Spin tracking simulations to investigate whether this special case generates spin rotations, which cannot be disentangled from the ones due a finite EDM by combining observations made with both counter-rotating beams as predicted by analytical derivations, will be presented.

Contents

1 Introduction

Several schemes to measure the Electric Dipole Moment (EDM) of charged particles are discussed at present [1, 2, 3, 4, 5, 6, 7]. Most of these proposals foresee to run a synchrotron satisfying the "frozen spin" condition. This condition requires that, in absence of an EDM and with the well known Magnetic Dipole Moment (MDM) in a perfect machine, bunches with initial longitudinal polarization (parallel or antiparallel to the direction of movement) remain longitudinally polarized. This implies that the spin of a reference particle (reference energy and reference orbit in perfect machine) rotates together with the direction of the trajectory. This is achieved by an appropriate choice of the electric and magnetic fields of bending elements. The effect of a finite EDM is a rotation of the spin around a radial direction from the longitudinal direction into the vertical direction. In an EDM ring the resulting vertical spin build up, which is very small for the smallest EDM to be detected in typical proposals, is measured with a polarimeter. The study presented here is for proposals based on a special case possibly only for particles with positive anomalous magnetic moment $G > 0$ as for example protons, is operation with beams at the "magic energy", where the "frozen spin" condition is met with only electric fields [2].

Systematic effects are any phenomena other than an EDM generating a vertical component of the polarization and limit the sensitivity, i.e. the smallest detectable EDM, of the proposed experiment. Such systematic effects may be generated by unwanted electric fields owing to imperfections in the focusing structure, such as misalignments of components, by magnetic fields penetrating the magnetic shielding or generated inside the shield (for example by the beam itself or the RF cavity), or gravity [3]. A combination of several such phenomena or a combination of an average horizontal polarization and one of these phenomena may also lead to such systematic effects. This paper describes a special case of systematic effects limiting the sensitivity of the experiment caused by transverse offsets of electrostatic bending elements and residual longitudinal magnetic fields inside the magnetic shieldings. The effect occurs both in purely electrostatic EDM rings and in hybrid rings with magnetic focusing. Simulations have been carried out for the symmetric hybrid ring proposal [8].

In most proposals (see, e.g., [3, 4, 8]), a target sensitivity of 10^{-29} e·cm is quoted, that corresponds to a vertical spin precession rate of 1 nrad/s for the 800 m circumference symmetric hybrid ring (this number will be useful throughout the work). Thus, any non EDM originating vertical spin precession rate larger than 1 nrad/s is considered a potential systematic error source.

We can distinguish between first order systematic effects and second order ones. First order effects, where one machine imperfection contributes to a vertical spin build up and second order effects, where instead two machine imperfections contribute to a vertical spin build up. In this paper, we will focus on a specific case of a second order effect, a geometric phase effect, due to horizontal offsets of bends and longitudinal magnetic fields penetrating the shield, described in Fig. 1. The horizontal offsets of bends will generate spin rotation in the horizontal plane due to the fact that the particle is no more at the magic energy while the longitudinal magnetic fields rotate the spin around the longitudinal axis generating a small vertical spin component. The fact that rotations are not commutative leads to a rotation around the radial axis, i.e., a typical geometric phase effect. Moreover, betatron oscillations

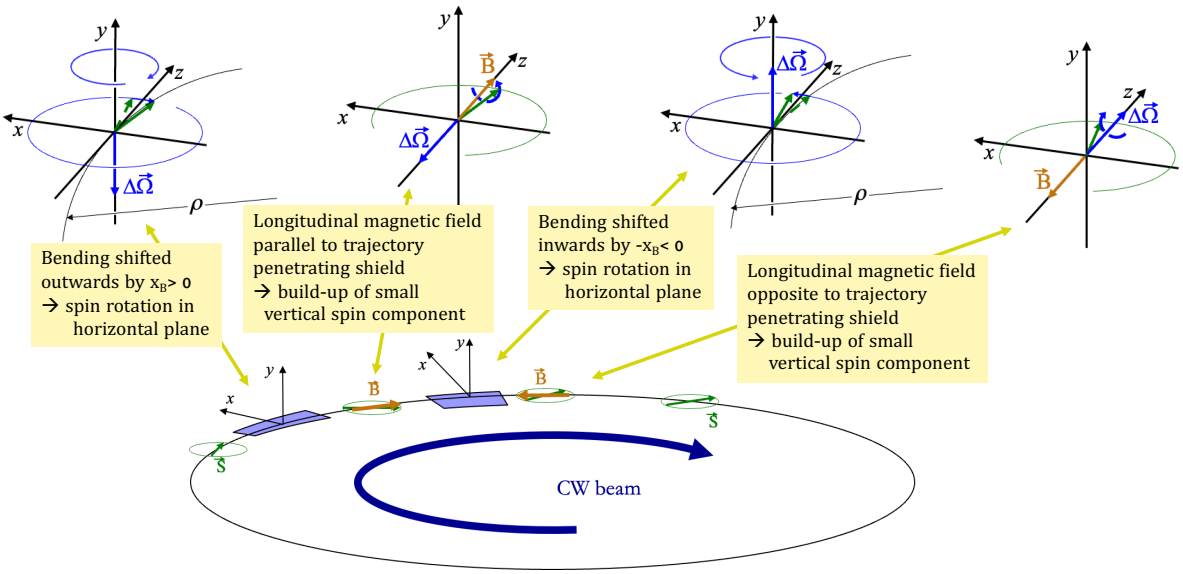

Figure 1: Detailed description of the mechanism of the geometric phase effect described in this paper.

are neglected with the analysis restricted to particles following the closed orbit.

2 Basic Equations and Magic Energy

The time evolution of the particle spin is described by the Thomas-BMT equation complemented by terms due to a possible EDM [9] as $d\vec{S}/dt = (\vec{\omega}_M + \vec{\omega}_E) \times \vec{S}$ and

$$\vec{\omega}_M = -\frac{q}{m}\left[\left(G+\frac{1}{\gamma}\right)\vec{B}_\perp + (G+1)\frac{\vec{B}_\parallel}{\gamma} - \left(G+\frac{1}{\gamma+1}\right)\vec{\beta}\times\frac{\vec{E}}{c}\right]$$

$$\vec{\omega}_E = -\frac{q}{m}\frac{\eta}{2}\left(\frac{\vec{E}_\perp}{c} + \frac{1}{\gamma}\frac{\vec{E}_\parallel}{c} + \vec{\beta}\times\vec{B}\right)$$

with $\vec{S}$ a (unit) vector pointing in the direction of the spin, $\vec{\omega}_M$ an angular frequency describing the particle with only an MDM and $\vec{\omega}_E$ an angular frequency describing spin rotation due an EDM. q and m are the particle charge and mass, γ and β the relativistic parameters and $\vec{B}$ and $\vec{E}$ the magnetic and electric fields. Indices $\perp$ and $\parallel$ denote the component perpendicular and parallel to the particles direction of motion. G is the anomalous magnetic moment factor and η describes a possible EDM. For protons with an EDM of $10^{-29}\, e\cdot$cm, these values are $G = 1.7928...$ and $\eta = 1.9\cdot 10^{-15}$.

For a magic energy ring, the angular frequency describing the rotation of the direction of motion along the reference orbit has only a vertical component given for a Clock-Wise (CW) beam by $\omega_{p,y} = -\beta c/\rho = (q/m)E_x/(\gamma\beta c)$ with ρ the bending radius. The angular frequency describing the rotation of the spin with an MDM only is $\omega_{M,y} = (q/m)(G+1/(\gamma+1))\beta E_x/c$. The frozen spin condition is satisfied for $\omega_{p,y} = \omega_{M,y}$ leading to the condition $\beta^2\gamma^2 = G^{-1}$.

The magic (kinetic) energy evaluated for protons is given by $E_m = (\sqrt{1+1/G}-1)m\,c^2 = 232.8\,\mathrm{MeV}$.

3 Geometric phase effect due to offset of bends and longitudinal magnetic fields

This study describes the BMAD [10] implementation of the symmetric hybrid ring lattice proposal and the study of a second order systematic effect: the geometric phase effect due to offset of bends and longitudinal magnetic fields. The symmetric hybrid ring design has been chosen for this study because it has interesting features, as the absence of spin rotation proportional to the unwanted magnetic fields due to focusing using magnetic quadrupoles. Anyway, it is necessary to take into consideration that, for this specific ring, the lattice is different for counter-rotating beams and thus the tuning is more delicate. More details on this lattice proposal can be found in [8] .

3.1 Analytical Estimates

The effect sketched in Fig. 1 for the simplified case simulated in Section 4.3 can be estimated by an analytical derivation. A horizontal offset of bend induces spin rotations around the vertical axis. In particular, we assume no deflection due to offset to simplify (deflection due to electrode spacing compensates and cannot be disentangled from offset). This offset generates a change of relativistic gamma by a bending offset of x_B that is $\Delta\gamma = -\frac{qE}{mc^2}x_B = \beta^2\gamma\frac{\alpha_B}{l_B}x_B$, where l_B is the length of the bending element and α_B is the bending angle. The angular frequency of spin rotation with respect to direction of:

$$\Delta\omega_y = \frac{q}{m}\left(G - \frac{1}{(\gamma+\Delta\gamma)^2-1}\right)\frac{\beta E_x}{c} = \frac{q}{m}\frac{2\gamma\Delta\gamma}{(\gamma^2-1)^2}\frac{\beta E_x}{c} = -2\frac{\beta}{\gamma}c\left(\frac{\alpha_B}{l_B}\right)^2 x_B.$$

The final change of radial spin is:

$$\Delta S_x = \frac{l_B}{\beta c}\Delta\omega_y = -\frac{2}{\gamma}\frac{\alpha_B^2}{l_B}x_B$$

and the radial spin component before and after the bending element is:

$$S_x = \pm\frac{1}{2}\Delta S_x.$$

An integrated magnetic field, instead, generates a rotation around the longitudinal axis and in particular a vertical spin per turn of:

$$\Delta S_y = 2\frac{l_B}{\beta c}\Delta\omega_z S_x = 2\frac{q}{m}\frac{G+1}{\beta\gamma c}B_s l_s S_x$$

and a build up rate of:

$$\frac{dS_y}{dt} = \frac{\Delta S_y}{C/\beta c}$$

where l_s is the length of the section where the magnetic field is applied, and B_s is the strength of the magnetic field.

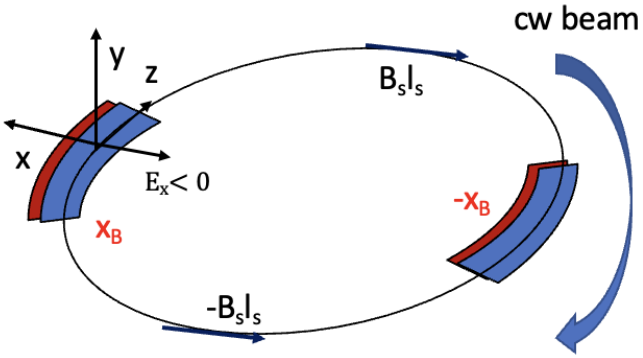

Figure 2: Example of the systematic effect studied and the BMAD reference system used to model the CW beam.

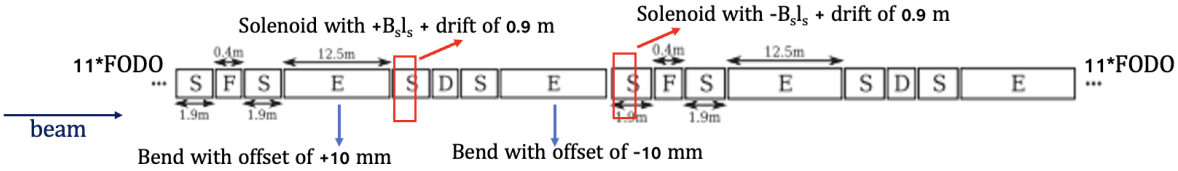

Figure 3: Schematic view of the lattice design and the systematic effect studied for this specific case (for the CW beam).

4 Simulation Results

The simulation results have been obtained with the BMAD tracking code. In the following, the implementation of the lattice for the Clock-Wise (CW) and Counter-ClockWise (CCW) beams is presented.

4.1 BMAD Lattice Implementation for the CW beam

Figure 2 shows an example of the schematic of the effect and the axis for the BMAD convention. An horizontal offset of the bends of $x_B = \pm 10$ mm has been added in two locations of the lattice as can be seen in Fig. 3. Then, the bending strengths has been adjusted to compensate the deflection due to the bending offsets, Moreover, a longitudinal magnetic field of 1,10,100 nTm has been added with solenoids (see Fig. 3). Then a correction of the energy to reduce the horizontal spin build up was performed.

The lattice functions can be seen in Fig. 4, where the Twiss parameters and the horizontal dispersion are shown.

4.2 BMAD Lattice Implementation for the CCW beam

The BMAD convention for the coordinate system has been applied, see example of the schematic of the effect and the axis in Fig. 5. Thus, the direction of the horizontal axis points inwards of the ring for the CCW beam. The sign of the horizontal electric field and

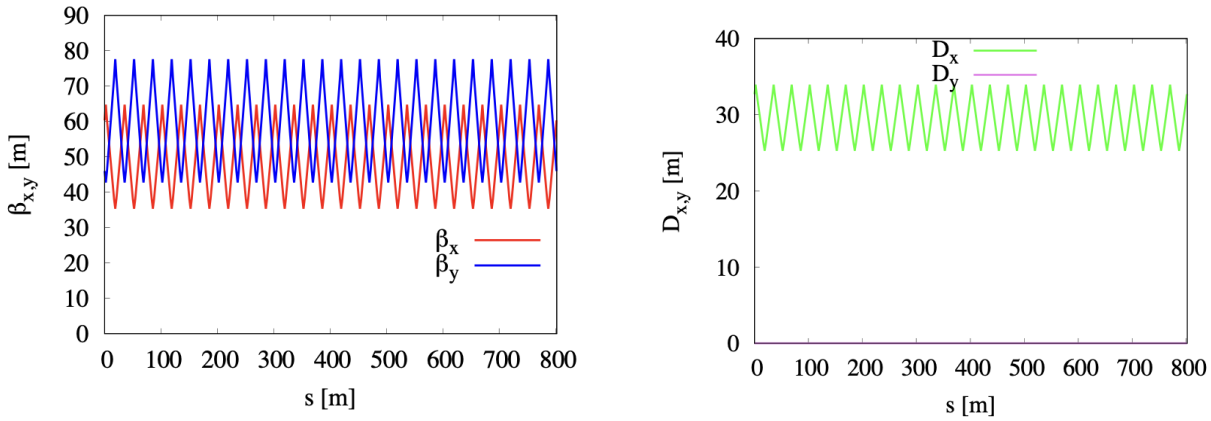

Figure 4: Twiss functions and horizontal dispersion for the CW beam.

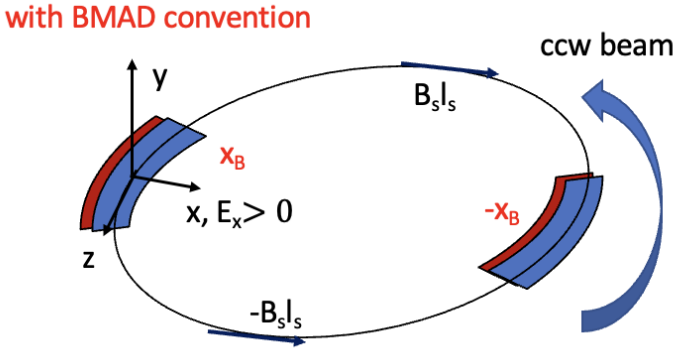

Figure 5: Example of the systematic effect studied and the BMAD reference system used to model the CCW beam.

the gradient of the magnetic quadrupoles are swapped. In order to implement the CCW beam in BMAD, the first step has been to invert the FODO cell, as can be seen in Fig. 6. The same systematic effects have been studied but with the beam passing before through the positive longitudinal magnetic field and the positive offset and after going towards the negative magnetic field and the negative offset (see Fig. 6).

The lattice functions can be seen in Fig. 7, where the Twiss parameters and the horizontal dispersion are shown.

4.3 Study of a simplified case

A simplified case studied here to understand the effect is generated by two bending offsets by ±10 mm interleaved in two locations with longitudinal magnetic fields (integrated fields of 0 nTm, ± 1 nTm, ± 10 nTm and ± 100 nTm).

The strength of the bendings is adjusted such that the deflection (corresponding, e.g., to a slight change of the electrode spacing) vanishes. In practice, independent positioning and strength errors will occur and generate orbit distortions resulting in additional systematic

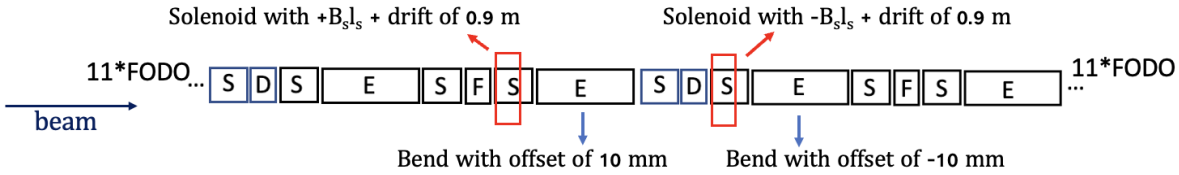

Figure 6: Schematic view of the lattice design and the systematic effect studied for this specific case (for the CCW beam).

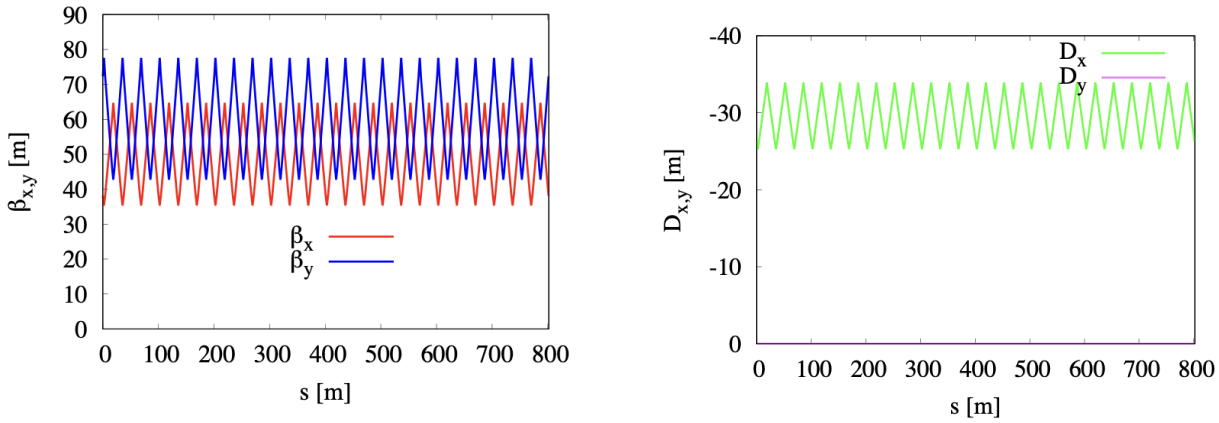

Figure 7: Twiss functions and horizontal dispersion for the CCW beam.

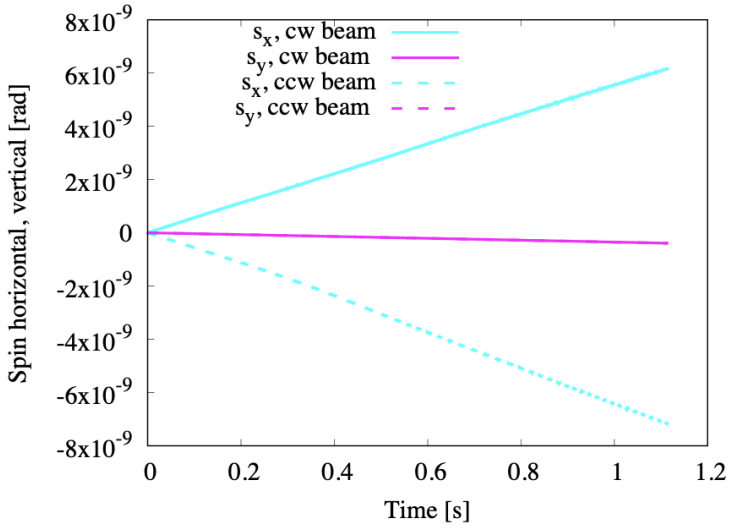

Figure 8: Horizontal and vertical spin build up for the CW and CCW beams with only the horizontal offsets of bends and no longitudinal magnetic fields.

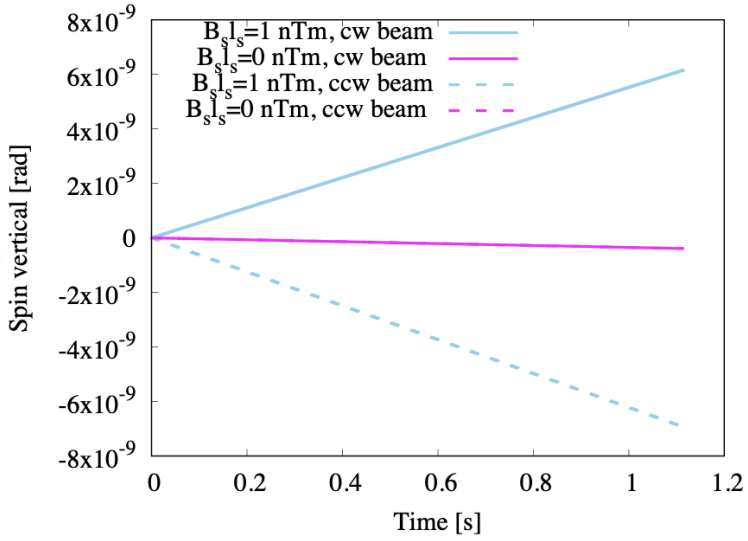

Figure 9: Vertical spin build up for the CW and CCW beams without longitudinal magnetic fields and with longitudinal magnetic fields of 1 nTm.

effects to be taken into account for a realistic sensitivity estimate. The effect is independent on the location of the machine imperfections provided bending offsets and longitudinal magnetic fields are interleaved. For the simulation presented here, all imperfections are located within a small portion of the ring. Simulations have been carried out for CW and CCW beams showing that, as expected, the effect cannot be disentangled from a finite EDM.

4.3.1 Simulation results for a longitudinally polarized beam

After implementing the bending offsets and without longitudinal magnetic fields, the particle energy has been slightly adjusted to reduce a slow spin rotation in the horizontal plane resulting in the spin evolution plotted in Fig. 8 for a proton initially polarized in longitudinal direction. The effect of adding weak integrated longitudinal magnet fields of $\pm$ 1 nT is shown in Fig. 9. Transverse spin components for a proton with initially longitudinal polarization for different additional integrated longitudinal magnetic fields in plotted in Fig. 10 and 11. One notes that the residual radial spin component after readjusting the particle energy is independent of the additional longitudinal magnetic fields. From Fig. 11, one observes that the vertical spin component generated by the effects agrees well with with analytical estimates and is as expected proportional to the additional longitudinal magnetic fields.

4.3.2 Simulation results for a radially polarized beam

Then, the simulations have been performed also for a beam with initial radial polarization to verify the absence of a spin rotation around the longitudinal axis due to finite integrated longitudinal magnetic field.

From Fig. 12, we can confirm the absence of spin rotation around the longitudinal axis for this specific case of systematic error. Additionally, the small vertical spin buildup is identical for all longitudinal magnetic fields and, thus, independent of them. The results

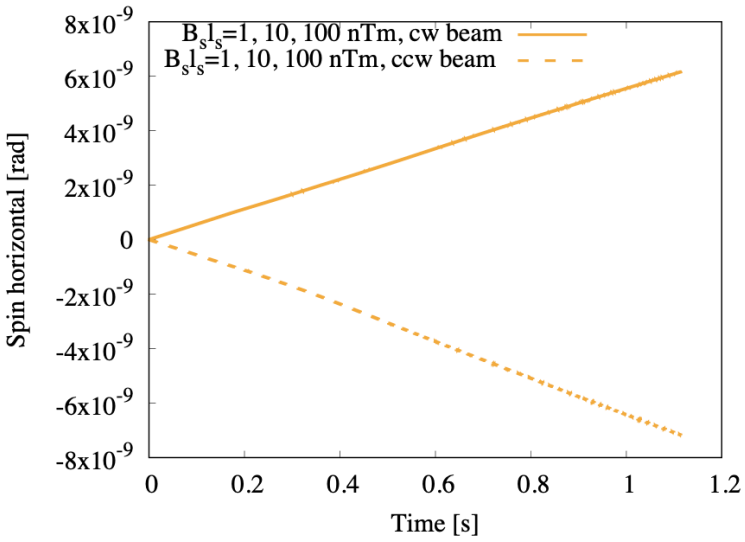

Figure 10: Horizontal spin build up for the CW and CCW beams with longitudinal magnetic fields of 1, 10, 100 nTm.

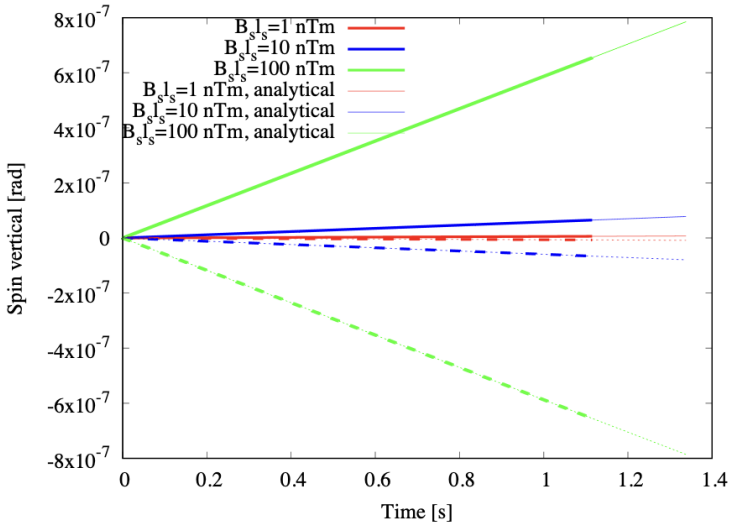

Figure 11: Vertical spin build up and comparison with analytical estimates for the CW and CCW beams with longitudinal magnetic fields of 1, 10, 100 nTm.

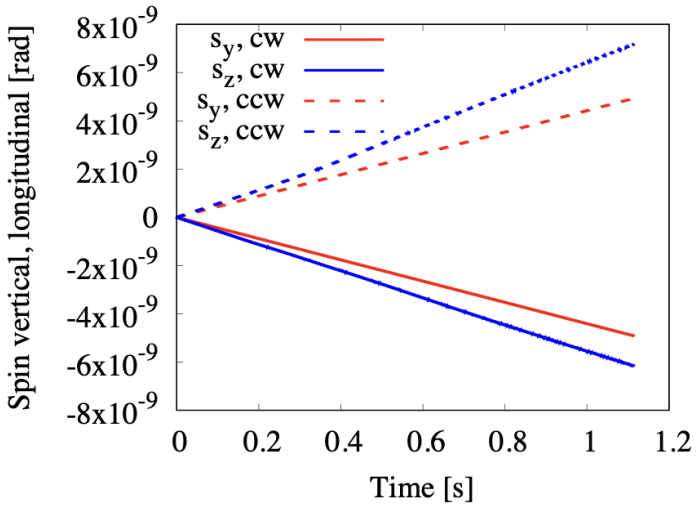

Figure 12: Vertical and longitudinal spin build up for the CW and CCW beams for a beam radially polarized.

presented cover all the longitudinal magnetic fields (integrated fields of 0 nTm, ± 1 nTm, ± 10 nTm, and ± 100 nTm), and the lines overlap because the vertical spin is the same for all the simulated cases. The slow rotation around the longitudinal axis of about ±5 nrad/s is then caused by numerical errors.

4.3.3 Comparison between simulations results and analytical estimates

A comparison between analytical estimates and simulation results has been performed using the formulas shown in Section 3.1.

In particular, a horizontal offset x_B=±10 mm of bends induces a change of radial spin $\Delta S_x = -22\mu$rad and a vertical spin $\pm S_x$=±11μrad at the bending exit and entrance, with the bending length of l_B=12.5 m and the deflection of $\alpha_B=\pi/24$. In Table 1 we can see a clear comparison between analytical estimates and simulation results, showing a very good agreement between them.

Table 1: Comparison between analytical estimates and simulation results for the simplified case.

Longitudinal field $B_S l_S$	S_y **per turn (analytical)**	S_y **per turn (simulations)**	**Build-up rate (analytical)**
1 nTm (CW beam)	2.60 $\times 10^{-14}$ rad	2.46 $\times$ 10^{-14} rad	5.9 nrad s^{-1}
10 nTm (CW beam)	2.60 $\times$ 10^{-13} rad	2.60 $\times$ 10^{-13} rad	59 nrad s^{-1}
100 nTm (CW beam)	2.60 $\times$ 10^{-12} rad	2.62 $\times 10^{-12}$ rad	590 nrad s^{-1}
1 nTm (CCW beam)	-2.60 $\times$ 10^{-14} rad	-2.77 $\times$ 10^{-14} rad	-5.9 nrad s^{-1}
10 nTm (CCW beam)	-2.60 $\times$ 10^{-13} rad	-2.63 $\times$ 10^{-13} rad	-59 nrad s^{-1}
100 nTm (CCW beam)	-2.60 $\times$ 10^{-12} rad	-2.62 $\times$ 10^{-12} rad	-590 nrad s^{-1}

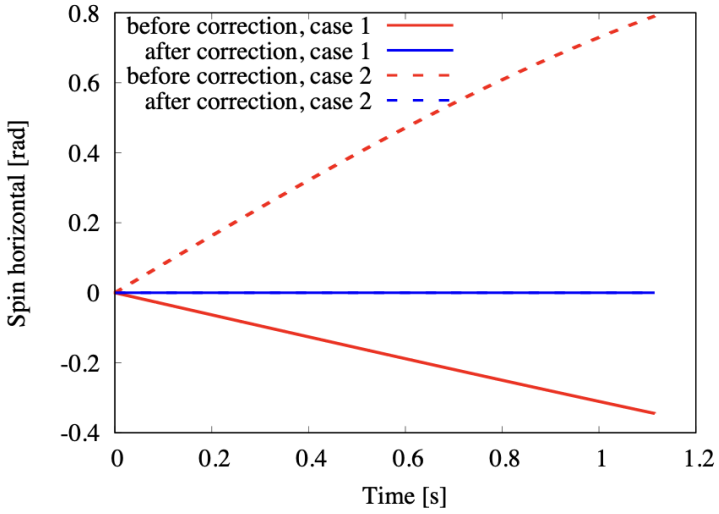

Figure 13: Horizontal spin build up before and after applying the energy correction for two different random seeds. The dashed blue lines are below the solid blue ones.

4.4 Study of a more realistic case

To understand the real limitation that can have this effect on the EDM measurement, a more realistic case has been studied. This involves a random offset of all the bendings with a reasonable small radial misalignment of 0.1 mm rms and reasonable longitudinal magnetic fields added with 48 solenoids with a length of 1 m and a random rms $k_S{=}B_s/B\rho$ value of 10^{-9} m^{-1}. In addition, the field of the bendings has again been adjusted (electrode spacing) to have no (or negligible) orbit deformation. Then, simulations have been done without any further correction and after adjusting the beam energy to strongly reduce a rotation in the horizontal plane and then setting the integrated longitudinal field to zero. The spin rotation in the horizontal plane is so large because the average of the bending offsets is not vanishing ($\bar{x}_B \neq 0$).

4.4.1 Simulation results for a longitudinally polarized beam

The results are shown for a longitudinally polarized beam and in addition different random seeds have been used for comparison (case 1 and case 2 in Fig. 13 and 14). Fig. 13 shows the horizontal spin build up before and after applying the energy correction. In fact, by applying the correction we can see that the horizontal spin build up goes very close to zero as we expect (the blue lines). Fig. 14 shows instead the vertical spin build up before and after applying the energy and the longitudinal magnetic field corrections (set the integral over one turn to zero). In fact, by doing that we can see that the effect from quadratic becomes linear as expected and it is equal to ≈ 3 nrad/s. Without corrections, the radial spin component increases about linearly with time (more precisely a sine wave). A non zero average longitudinal magnetic field leads to a small rotation of this radial component into the vertical direction leading to a contribution increasing quadratically with time (more precisely proportional to a cosine function), as represented by the purple traces in Fig. 14.

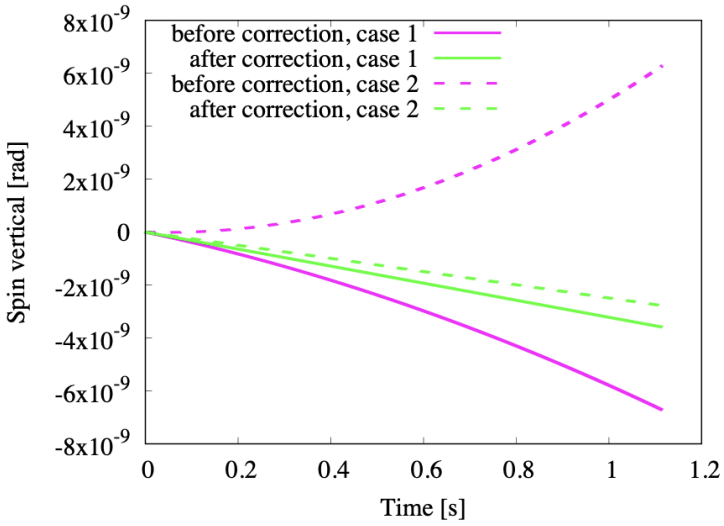

Figure 14: Vertical spin build up before and after applying the energy and the longitudinal magnetic field correction for two different random seeds.

4.4.2 Simulation results for a radially polarized beam

Then, also in this case, the simulations have been performed also for a beam with initial radial polarization to verify the absence of a spin rotation around the longitudinal axis due to finite integrated longitudinal magnetic field.

From Figs. 15, 16 we can confirm, also in this case, the absence of a spin rotation around the longitudinal axis for this specific case of systematic error and that the small vertical spin build up is the same for all longitudinal magnetic fields and, thus, independent of them. Also in this case, there is again a small rotation around the longitudinal axis probably caused by numerical errors.

5 Conclusion

Geometric phase effects caused by offsets of bendings and residual longitudinal magnetic fields inside the shield have been studied. The offset of the bendings generate spin rotation in horizontal plane while the longitudinal magnetic fields generate rotations around longitudinal axis. The net effect is a rotation around the radial axis that rotates the longitudinal spin component into the vertical direction. It has been shown that this effect mimics a finite EDM (cannot be disentangled from EDM combining observations with CW and CCW beams). It has also been shown that there are no net rotation around the longitudinal axis rotating radial spin component into the vertical direction.

From the simulations for the more realistic case, possibly with still optimistic assumptions, for a longitudinally polarized beam there is a geometric phase effect of ≈ 3 nrad/s, 3 times larger than what an EDM of 10^{-29} e·cm would give. In practice, bending elements will have integrated strength errors and radial position offsets. Both generate closed orbit perturbations, which cannot be disentangled. As consequence, there will be spin rotations in the horizontal plane which do not correlate with orbit perturbations, which could be

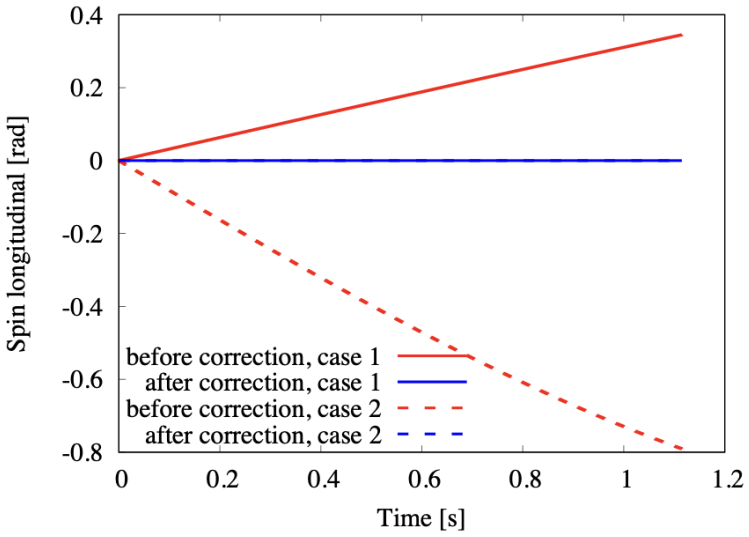

Figure 15: Longitudinal spin build up for a beam radially polarized before and after applying the energy and the longitudinal magnetic field correction for two different random seeds. The dashed blue lines are below the solid blue ones.

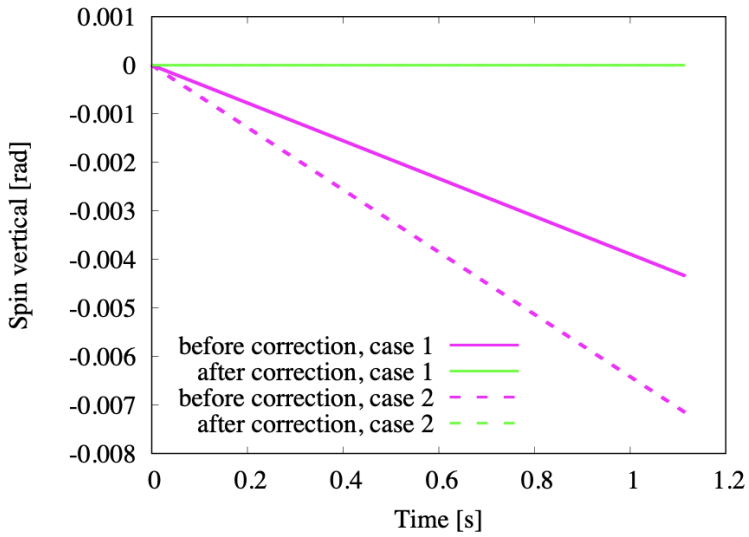

Figure 16: Vertical spin build up for a beam radially polarized before and after applying the energy and the longitudinal magnetic field correction for two different random seeds.

measured and used for mitigation measures. The effect occurs for any frozen spin machine and not only the symmetric hybrid lattice [8] used for simulations. This is an example of a geometric phase effect that cannot be disentangled from a finite EDM by combining spin rotations made with both counter-rotating beams.

References

[1] F.J.M. Farley, K. Jungmann, J.P. Miller, W.M. Morse, Yu F. Orlov, B.L. Roberts, Yannis K. Semertzidis, A. Silenko, and E.J. Stephenson. New method of measuring electric dipole moments in storage rings. *Physical review letters*, 93(5):052001, 2004.

[2] V. Anastassopoulos, S. Andrianov, R. Baartman, S. Baessler, M. Bai, J. Benante, M. Berz, M. Blaskiewicz, T. Bowcock, K. Brown, et al. A storage ring experiment to detect a proton electric dipole moment. *Review of Scientific Instruments*, 87(11), 2016.

[3] Falastine Abusaif, Anjali Aggarwal, A Aksentev, B Alberdi-Esuain, A Andres, A Atanasov, L Barion, S Basile, M Berz, C Böhme, et al. Storage ring to search for electric dipole moments of charged particles–feasibility study. *arXiv preprint arXiv:1912.07881*, 2019.

[4] V. Anastassopoulos et al. A proposal to measure the proton electric dipole moment with 10^{-29} e·cm sensitivity. *by the Storage Ring EDM Collaboration*, 2011.

[5] Yury Senichev, S. Andrianov, A. Ivanov, S. Chekmenev, Martin Berz, and Eremey Valetov. Investigation of lattice for deuteron EDM ring. In *Proceedings of ICAP*, pages 17–19, 2015.

[6] Alexander Skawran and Andreas Lehrach. Spin tracking for a deuteron EDM storage ring. In *Journal of Physics: Conference Series*, volume 874, page 012050. IOP Publishing, 2017.

[7] A.E. Aksentev and Y.V. Senichev. Frequency domain method of the search for the electric dipole moment in a storage ring. In *Journal of Physics: Conference Series*, volume 1435, page 012047. IOP Publishing, 2020.

[8] Zhanibek Omarov, Hooman Davoudiasl, Selcuk Hacıömeroğlu, Valeri Lebedev, William M. Morse, Yannis K. Semertzidis, Alexander J. Silenko, Edward J. Stephenson, and Riad Suleiman. Comprehensive symmetric-hybrid ring design for a proton EDM experiment at below $10^{-29}\mathrm{e}\cdot\mathrm{cm}$. *Phys. Rev. D*, 105:032001, Feb 2022.

[9] Takeshi Fukuyama and Alexander J. Silenko. Derivation of generalized Thomas-Bargmann-Michel-Telegdi equation for a particle with electric dipole moment. *International Journal of Modern Physics A*, 28(29):1350147, 2013.

[10] BMAD: Software Toolkit for Charged-Particle and X-Ray Simulations.